Apoptosis (2016) 21:1106–1124
DOI 10.1007/s10495-016-1268-8

Mephebrindole, a synthetic indole analog coordinates the crosstalk between p38MAPK and eIF2α/ATF4/CHOP signalling pathways for induction of apoptosis in human breast carcinoma cells

Supriya Chakraborty[1] · Swatilekha Ghosh[1] · Bhaswati Banerjee[1] · Abhishek Santra[1] · Jyotsna Bhat[2] · Arghya Adhikary[3] · Subhrangsu Chatterjee[2] · Anup K. Misra[1] · Parimal C. Sen[1]

Published online: 8 July 2016

Abstract The efficacy of cancer chemotherapeutics is limited by side effects resulting from narrow therapeutic windows between the anticancer activity of a drug and its cytotoxicity. Thus identification of small molecules that can selectively target cancer cells has gained major interest. Cancer cells under stress utilize the Unfolded protein response (UPR) as an effective cell adaptation mechanism. The purpose of the UPR is to balance the ER folding environment and calcium homeostasis under stress. If ER stress is prolonged, tumor cells undergo apoptosis. In the present study we demonstrated an 3,3′-(Arylmethylene)-bis-1*H*-indole (AMBI) derivative 3,3′-[(4-Methoxyphenyl) methylene]-bis-(5-bromo-1*H*-indole), named as Mephebrindole (MPB) as an effective anti-cancer agent in breast cancer cells. MPB disrupted calcium homeostasis in MCF7 cells which triggered ER stress development. Detailed evaluations revealed that mephebrindole by activating p38MAPK also regulated GRP78 and eIF2α/ATF4 downstream to promote apoptosis. Studies extended to in vivo allograft mice models revalidated its anti-carcinogenic property thus highlighting the role of MPB as an improved chemotherapeutic option.

Keywords Breast cancer · Calcium · Unfolded protein response · ER stress · p38MAPK · Reactive oxygen species

Abbreviations

MPB	Mephebrindole
UPR	Unfolded protein response
ER stress	Endoplasmic reticulum stress
GRP78	Glucose regulated protein 78
ATF4	Activating transcription factor 4
CHOP	CCAAT-enhancer-binding protein homologous protein
eIF2α	Eukaryotic initiation factor 2α
ChIP	Chromatin immunoprecipitation
p38 MAPK	p38 Mitogen activated protein kinase
AMBI	Aryl methyl bis-indolyl derivative
NAC	*N*-Acetyl cysteine

Introduction

The importance of the unfolded protein response (UPR) in the maintenance of malignancy has inspired great interest in exploring the therapeutic potential of targeting UPR components. Tumor cells grow under oncogenic stress caused by hypoxia, nutrient deprivation, DNA damage [1] metabolic and oxidative stress, leading to UPR as an adaptation strategy. However, most normal cells are not subjected to stress and the UPR pathways remain inactive in these cells. The difference between tumor and non-tumorogenic cells thus offer an advantage of targeting the UPR to achieve specificity in cancer therapy [2]. If tumor

Electronic supplementary material The online version of this article (doi:10.1007/s10495-016-1268-8) contains supplementary material, which is available to authorized users.

✉ Parimal C. Sen
parimal@jcbose.ac.in; parimalsen.boseinst@gmail.com

[1] Division of Molecular Medicine, Bose Institute, P-1/12, Calcutta Improvement Trust Scheme VII M, Kolkata 700 054, India

[2] Department of Biophysics, Bose Institute, P-1/12, Calcutta Improvement Trust Scheme VII M, Kolkata 700 054, India

[3] Centre for Research in Nanoscience and Nanotechnology, University of Calcutta, Kolkata, India

cells are exposed to another form of ER stress, the intensity of the stress might be a threshold, thereby inducing specific cell death in tumor cells, with less effect on non-tumorogenic cells. ER stress inducing mechanisms are also potential anti-cancer strategies through disturbing the adaptive response of UPR. Therefore increasing misfolded proteins in ER to overload protein folding requirements, inducing more severe ER stress and cell death, lead to increased sensitivity of anticancer therapy [3].

The UPR is a cellular adaptive response that evolved to restore protein folding homeostasis through phosphorylation of eIF2α and by increasing the ER protein folding and degradation capacities through transcriptional activation of XBP1 and ATF6 [4–6]. If the UPR cannot resolve the protein folding defect, cells underwent apoptosis. One of the mechanisms of ER stress induced cell death involves sequential steps of GRP78 mediated eIF2α phosphorylation [7, 8], preferential translation of ATF4 messenger RNA [9–11] and induction of CHOP/GADD153 [12–14]. This ATF4 and CHOP-dependent cell autonomous apoptosis may have evolved to selectively eliminate stress damaged or infected cells from the organism. Thus identification of small molecules that can target the UPR in cancer cells might be effective in development of anti-cancer therapy.

Some plants and fungi are rich in indole-containing molecules which include indole-3-carbinol (I3C), harmane, lysergic acid, bufotenin, serotonin, tryptamine etc. In contrast, the anticancer potential of indole derivatives present in vegetables is still largely unknown. Indole 3-carbinol is a key bioactive molecule of cruciferous vegetables and well explored for prevention of few type of cancers (colorectal, lymphoma, breast, trans-placental cancer in offspring and prostate cancer [15, 16]. Ingested I3C can be converted into a biologically active dimer, 3,3-diindolylmethane (DIM), within the gastrointestinal tract. Since DIM accumulates in the cell nucleus, it likely contributes to cell nuclear events that have been ascribed to I3C. Several mechanisms may account for the anticancer properties of I3C/DIM including changes in cell cycle progression, apoptosis, carcinogen bioactivation and DNA repair [17, 18]. Despite these advances in translational research, the mechanism by which I3C/DIM inhibits tumorogenesis remains inconclusive, this, in part, might be attributable to its metabolic instability and complicated pharmacological properties. From a mechanistic perspective, the ability of 13C/DIM to target a broad spectrum of signaling pathways underlies their anti-proliferative effects. However, these agents suffer from metabolic instability, unpredictable pharmacokinetic properties, and low in vitro anti-proliferative potency, which render therapeutic concentrations difficult to achieve in the body. Consequently, recent years have witnessed the use of diindoylmethanes as a scaffold to carry out structural modifications, which has led to distinct antitumor agents with higher potency reported in the literature: SR13668 (an Akt inhibitor) [18], and an indole-3-carbinol tetrameric derivative [17], *N*,*N*′-glycoside derivatives of 3,3′-diindolylmethanes derivative [19], and aryl methyl bis indolyl derivative (AMBI). These new agents exhibited μmol/L potency in inducing apoptosis, however, the signaling pathways affected by them is are distinctly different from those that are regulated by their parent molecule, diindoylmethanes.

In the present study, we have reported the use of DIM as a lead compound to develop antitumor agents with improved chemical stability and apoptosis-inducing potency. This structural optimization effort culminated in the generation of 3,3′-[(4-methoxyphenyl) methylene]-bis-(5-bromo-1*H*-indole) named as mephebrindole, a stable DIM analogue with two orders of magnitude higher apoptosis-inducing capacity than the parental diindoylmethanes. Moreover, mephebrindole retained the pleiotropic effects of DIM on multiple signaling targets associated with growth arrest and apoptosis. Mephebrindole in one hand causes calcium imbalance in breast cancer cells, on the other hand it activates p38 MAPK. These two factors regulate ER stress and activate UPR adaptation in breast cancer cells. Due to simultaneous regulation of these two factors in presence of mephebrindole, it resulted in the generation of prolonged ER stress in cancer cells. UPR thus becomes unable to compensate this and turned on the pro apoptotic cascade via eIF2α/ATF4 mediated CHOP activation. This led to reactive oxygen species accumulation in cancer cells and triggered mitochondria dependent apoptotic cascade leading to substantial death in breast cancer cells. Despite this broad spectrum of pharmacologic activities, mephebrindole left the normal breast epithelial cells and the peripheral blood mononuclear cells significantly unaffected. In fact the efficacy of the compound was also further justified from the tumor regression in vivo mice model. Cumulatively, our study thus reports for the first time an intricate mechanism of MPB mediated cancer regression in breast cancer cells and also suggests its role as a possible therapeutic agent to treat breast cancer patients.

Materials and methods

Cell culture

MCF7, HBL100, T47D cell lines were obtained from NCCS, Pune, India. Cells were routinely maintained in Dulbecco's Modified Eagle Medium DMEM (HiMedia) supplemented with 10 % FBS (GIBCO) at 37 °C in a humidified incubator with 5 % CO_2. All stock solution of

compounds were prepared in cell culture grade DMSO and stored in room temperature. Compounds were diluted in culture media prior to use in experiments. MCF-10A cells were cultured in F12/DMEM (Gibco) with 10 % serum (Gibco), 5 ng/mL epidermal growth factor (SIGMA), 10 μg/mL insulin (SIGMA), 0.1 μg/mL cholera toxin (SIGMA), 0.5 μg/mL hydrocortisone (SIGMA).

Chemical synthesis and characterization of indole analogues

In order to develop an environmentally benign aqueous reaction condition for the preparation of 3,3′-(aryl methylene)-bis-(1*H*-indole) (AMBI) derivatives, aluminium dodesylsulfate has been chosen as a catalyst because of its ability to form micelles in water together with its catalytic potential reported earlier [20]. Following the literature report $[Al(DS)_3]\cdot 3H_2O$ (white powder) was prepared by the reaction of aluminium nitrate nonahydrate and sodium dodecyl sulfate in water at room temperature. In a set of initial experiments, 4-chlorobenzaldehyde (1 mmol) was allowed to react with 1*H*-indole (3 equiv.) in water (5 mL) in the presence of a varied quantities of $[Al(DS)_3]\cdot 3H_2O$ (0.1–0.5 equiv.) as catalyst at room temperature. The reaction mixture became turbid on stirring at room temperature and 3,3′-(4-chlorophenylmethylene)-bis-(1*H*-indole) (compound 3) was formed with 90 % yield. After a series of experimentation it was observed that reaction of 4-chlorobenzaldehyde with 2.2 equivalent of 1*H*-indole in water (5 mL) in the presence of $[Al(DS)_3]\cdot 3H_2O$ (0.1 equiv.) could furnish compound 3 in 90 % yield. In order to generalize the reaction condition a series of aromatic aldehydes were treated with variety of indole derivatives under similar reaction conditions and excellent yield (82–92 %) of the 3,3′-(arylmethylene)-bis-(1*H*-indole) (AMBI) derivatives (compounds, 1–20) were achieved in every case. Results are presented in Supplementary file 3. After completion of the reaction (monitored by TLC) the reaction product was extracted with diethyl ether. The aqueous solution containing the catalyst can be reused for five times without noticeable decrease in the catalytic potential. Most of the AMBI derivatives were obtained as solid products, which were characterized by their melting points and spectral analysis. Aromatic aldehydes containing electron donating and withdrawing functional groups furnished AMBI derivatives in similar yields. It has been observed that stirring of the aqueous reaction mixture play important role in the yield of the product formation since very low yield of the product was formed if the reaction mixture was kept for a long time without stirring. Spectral data of the compounds are available in Supporting information (Supplementary file 1 and 2). Here we only provided the details of most effective molecule mephebrindole (MPB). Chemical name: 3,3′-[(*p*-methoxyphenyl)methylene]-bis-(5-bromo-1*H*-indole).

m.p.: 246-248 °C [EtOH]; IR (KBr): 3411, 1611, 1506, 1458, 1419, 1262, 1217, 1164, 1014, 743 cm^{-1}; ^1H NMR (500 MHz, $CDCl_3$): δ 7.98 (br s, 2 H, 2 H-4), 7.44 (br s, 2 H, 2 H-7), 7.25–7.15 (m, 4 H, 2 × H-6, H-2′,6′), 6.82 (d, $J = 8.5$ Hz, 2 H, 2 × H-2), 6.59 (br s, 2 H, H-3′,5′), 5.68 (s, 1 H, CH), 3.79 (s, 3 H, OCH_3), 11.23 (2H, br s, 2 × NH); ^{13}C NMR (125 MHz, $CDCl_3$): δ 158.1, 135.4, 129.4 (4 C), 128.6, 125.0 (2 C), 124.6 (2 C), 122.3 (2 C), 119.4 (2 C), 113.8 (4 C), 112.7, 112.5 (2 C), 55.1 (OCH_3), 39.0 (CH); ESI–MS: 509.0 $[M+1]^+$; Anal. Calcd. for $C_{24}H_{18}Br_2N_2O$ (510.22): C, 56.50; H, 3.56; found: 56.42; H, 3.64.

Antiproliferative activity

For general anticancer screening and also for other biochemical assay, compounds was dissolved in DMSO. The final concentration of DMSO never exceeded 1 % of the total reaction volume. A set of 20 compounds have been screened against different cancer cell lines. The effect of these compounds on cancer cell death was assessed by MTT assay. Briefly, cancer cells were plated in 96 well plates and allowed to grow at 37 °C for overnight. Next day the cells were treated with compounds in different concentrations for 24 h. Following 24 h treatment cell media was replaced by MTT containing media (0.5 mg/mL) and incubated at 37 °C for 3 h. After that DMSO was added to the cells, to dissolve the MTT crystal, absorbance was measured in an ELISA reader (Bio-Rad) at 570 no.

Annexing V-PI staining

For the determination of cell death, cells were stained with presidium iodide and annexing-V-FITC (BD Pharmingen, CA, USA) and analyzed by flow cytometry, (FACS Calibur, Beckton Dickinson, CA, USA) equipped with 488 nm argon laser light source, using Cell Quest Software (BD Biosciences, CA, USA). Electronic compensation of the instrument was done to exclude overlapping of the emission spectra. Total 10,000 events were acquired for analysis using Cell Quest software. Annexin-V-PI positive cells were regarded as apoptotic cells.

Detection of mitochondrial membrane potential and intracellular reactive oxygen species (ROS) generation

The changes in mitochondrial membrane potential were determined using JC1 (Molecular probes). Cells were treated with DMSO or mephebrindole for indicated time periods, harvested, washed twice in PBS, resuspended in

PBS supplemented with JC1 (20 nM), incubated at 37 °C for 15 min in the dark, and immediately analyzed by flow cytometry or fluorescence microscope. The intracellular accumulation of ROS was examined by flow cytometry after being stained with the fluorescent probe, 2,7-dichlorodihydro-fluorescein diacetate (DCFH-DA; molecular probes) (10 μM). DCFH-DA was deacetylated in cells by esterase to a non-fluorescent compound, DCFH, which remains trapped within the cell and is cleaved and oxidized by ROS in the presence of endogenous peroxidase to a highly fluorescent compound, 2,7-dichlorofluorescein (DCF). Briefly, MCF7 cells were seeded in 6-well plates (5×10^5 cells/mL), treated with or without MPB and other compounds for different time periods, and incubated with 10 μM DCFH-DA for 30 min at 37 °C. Cells were washed, resuspended in PBS, and ROS levels were determined using FACS Calibur flowcytometry.

$[Ca^{2+}]_c$ measurements using a fluorescence microplate reader

This method as reported by Robinson et al. [21] was followed. For $[Ca^{2+}]_c$ measurement, MCF-7 cells were seeded onto 96-well plates at a density of 2500 cells/well in 100 μL of growth media. At sub confluence, the culture medium was replaced with FBS free media for 24 h to attempt to synchronize cells into a non proliferative stage. MCF-7 cells were then loaded with 2.5 μM fluo-3/AM in medium at 37 °C for 30 min followed by 30 min at room temperature to minimize dye leakage and sequestration into intracellular organelles. After loading, cells were washed twice with 200 μL HBSS (in order to remove excess fluorescent dye). Cells were then treated for different durations with different compounds in normal or calcium-free medium. Cells were washed twice with 200 μL HBSS and then 100 μL HBSS/well was added. The fluorescence intensity of fluo-3 was measured at an excitation wavelength of 485 nm and an emission wavelength of 520 nm. Relative changes in calcium concentration using fluo-3 were determined by calculations of $\delta F/F_0$, where $\delta F/F_0 = (F_t - F_0)/F_0$. Ft represents the fluorescence reading at each time point and F_0 the initial fluorescence.

$[Ca^{2+}]_c$ measurements using a FACS

MCF7 cells were trypsinized, washed, placed in Eppendorf tubes at 1×10^6/mL, and incubated with 3 μM of Fluo-3AM (Molecular Probes) in 3 % DMSO at 37 °C in complete DMEM for 30 min. Fluo-3 AM is a high-affinity calcium indicator with $\lambda ex = 470–490$ nm and $\lambda em = 520–540$ nm. After incubation, cells were washed three times with Ca^{2+}/Mg^{2+} PBS (Sigma-Aldrich) by centrifugation (1 min at $300 \times g$ or 1700 rpm), and resuspended in Ca^{2+}/Mg^{2+} PBS. Fluorescence data was collected and analyzed on the BD Accuri in FL1 using a 530/30 BP filter or, when the signal was too bright, a 585/40 BP filter, which can detect about 10 % of the signal. Baseline calcium levels were recorded for 60 s on the BD Aria followed by the addition of 10 μM of thapsigargin (TG), 25 μM of ionomycin (all from Santa Cruz Biotechnology, USA). All compounds were added and mixed using a gel loading pipet tip. At the end of each test, 25 μM of ionomycin was added to each sample as a positive control. In some experiments, 80 μM of EGTA (Sigma-Aldrich) was added as a negative control or to provide calibration curves. To ensure that the addition and mixing of compounds did not interfere with data collection, additional control conditions were maintained. Fresh sample was removed or added or mixed with the cell suspension, and air bubbles were introduced into the sample with an empty pipet [22, 23].

Immunoblotting

MCF7 cells were lysed in buffer (10 mM Hepes, pH 7.9, 1.5 mM $MgCl_2$, 10 mM KCl, and 0.5 mM DTT) and nuclei were pelleted by brief-centrifugation. The supernatant was spun at $100{,}000 \times g$ to get cytosolic fraction. The nuclear extract was prepared in buffer containing 20 mM HEPES, pH 7.9, 25 % (v/v) glycerol, 420 mM KCl, 1.5 mM $MgCl_2$, 0.2 mM EDTA, 0.5 mM DTT, and 0.5 mM PMSF. All buffers were supplemented with protease and phosphatase inhibitor cocktails. For direct western blot analysis, cell lysates of the particular fractions containing 30 μg protein were separated by SDS–polyacrylamide gel electrophoresis and transferred to PVDF membrane. The protein levels of GRP78 (Sigma, USA), ATF4, CHOP cleaved caspase9 and cleaved PARP, phosphop38, BAX, BCL-2 were determined with specific antibodies. The protein of interest was visualized by chemiluminescence. Equal protein loading was confirmed by reprobing the blots with β-actin/GAPDH antibody. MCF7 cells were treated with 10 μM mephebrindole for different time periods, harvested and used for isolation of mitochondrial and cytosolic fractions using mitochondrial extraction kit (IMGENEX, USA, Cat. No. 10082k) as per the manufacturer's instructions. DMSO treated cells were used as control. The resulting fractions were used for western blot analysis against anti-cytochrome *c* (All antibodies used in the experiments were obtained from Santa Cruz Biotechnology, USA).

Fluorescence/confocal imaging

For the identification of subcellular expression of ATF4 under different conditions, the MCF7cells were fixed and

permeabilised with 100 % chilled methanol for 7 min. Cells were then stained with anti cytochrome *c* and anti ATF4 antibody followed by FITC-conjugated secondary antibody and visualized with fluorescence light microscopes (Leica Microsystem). For live cell imaging of calcium, MCF7 cells were treated with mephbrindole for different time periods and incubated with fluo-3AM in Hanks' buffered saline solution for 30 min followed by visualisation with BD Pathway microscope.

Cytochrome *c* was detected in MCF-7 cells cultured on 12-mm diameter round coverslips overnight and then incubated with freshly titered mito-Tracker, usually 80 nM, (molecular probes) in pre warmed culture medium for 30 min at 37 °C for labeling. The coverslips were washed three times with HBSS and soaked in 80 µL of HBSS containing 10 mM Hepes, 2 mM $CaCl_2$, and 4 mg/mL BSA. The cells were fixed in 3.7 % formaldehyde-PBS for 10 min. The cells were washed three times with PBS and incubated with mouse monoclonal anti–cytochrome *c* antibody (Santa Cruz) diluted in PBS containing 10 % BSA and 0.1 % NP-40 for 1 h at room temperature with agitating. After washing three times with PBS, the cells were incubated with TRITC goat anti–mouse antibody (Sigma-Aldrich) diluted in the same buffer for 1 h. The cells were washed three times in PBS and mounted with 3 µL of antifade reagent with DAPI (VECTASHIELD) on a glass slide. Image analysis was performed using Zeiss's Confocal microscope.

Reverse transcriptase and qRT PCR

Total RNA was estimated using a semiquantitative reverse transcriptase-PCR method. Briefly, total RNA from cells was extracted with TRIZOL reagent (SIGMA) as described previously [24]. Reverse transcription was performed using Verso CDNA synthesis kit (Thermo Scientific). PCR was performed using PCR master Mix (Biobharati). Sequences for PCR primers are described in Supplementary Table 3.

qRT-PCR was performed with 50 µg sample using Light cycler 96 (Roche) and FastStart Universal SYBR Green Master (Roche) and specific primers (Supplementary Table 3) and glyceraldehyde-3-phosphate dehydrogenase (GAPDH) was used as internal controls for mRNA quantification. Gene expression was defined from the threshold cycle (Cq), and relative expression levels were calculated by using the $2^{-\Delta Cq}$ method after normalization with reference to expression of housekeeping genes (GAPDH).

Chromatin immunoprecipitation (ChIP) assay

Chromatin immuno-precipitation assay was performed using ChIP assay kit (Millipore) following manufacturer's instructions. Isolated chromatin was precipitated with ATF4 antibody. Input DNA, rabbit IgG-pulled DNA served as controls for all the experiments. Immunoprecipitated DNA was then subjected to 35 cycles of PCR using primers for respective CHOP promoter region (Supplymentary Table 3 for primers sequence). Glyceraldehyde-3-phosphate dehydrogenase (GAPDH) promoter was used as a nonspecific control for all the ChIP experiments. The results were normalized to the chromatin input of the IP.

siRNA and transfection

MCF7 cells were plated In a six well tissue culture plate, (seeded 2×10^5 cells per well) in 2 mL antibiotic-free normal growth medium supplemented with FBS. Cells were incubated at 37 °C in a CO_2 incubator for overnight. Next day 80 % confluent cells were transfected with 300 pmol (each well 50 pmol) CHOP siRNA (Santa Cruz Biotechnology) and lipofectamine 2000 (Invitrogen, Carlsbad, USA). Control siRNA was purchased from Santa Cruz Biotechnology, USA(Sc-37007) that contain a scrambled sequence that will not lead to the specific degradation of any known cellular mRNA. Levels of respective protein were estimated by Western blotting.

Animals

All ethical guidelines of the animal ethics committee of the Institute (Ref no: 1796/GO/EReBiBt/S/14/CPCSEA) for handling and performing of the experiments were followed. Swiss albino female mice, 6–8 weeks old, weighing 18–22 g were purchased from Chittaranjan National Cancer Institute, Kolkata and acclimatized in the Institute animal house before experiments started. The animals were housed in polypropylene cages and provided standard pellet diet (Agro Corporation Pvt. Ltd., India) and water. The standard pellet diet composed of 21 % protein, 5 % lipids, 4 % crude fiber, 8 % ash, 1 % calcium, 0.6 % phosphorus, 3.4 % glucose, 2 % vitamin, and 55 % nitrogen-free extract (carbohydrates). The mice were maintained under controlled conditions of temperature and humidity with a 12 h light/dark cycle.

Preparation of Ehrlich ascites carcinoma (EAC) cells

EAC cells were collected from the peritoneal cavity of tumor-bearing donor mice of 20–22 g body weight and suspended in sterile phosphate buffered saline (PBS). A fixed number of viable cells (1.0×10^6 cells/20 g body wt) were implanted into the peritoneal cavity of each recipient mouse and allowed to multiply. The tumor cells were withdrawn, diluted in saline, counted and re-injected to

thigh tissue of experimental animals for developing solid tumor.

Treatment of animals

Female Swiss albino mice (20 g) were randomly divided into Three groups of 10 animals each which consist of (i) EAC bearing set, (Untreated), (ii) 10 mg/Kg body weight MPB-treated tumor bearing set, (iii) 20 mg/Kg body weight MPB treated tumor bearing set. Untreated mice received DMSO instead of MPB. After injection of the tumor cells, it took about 4 days for tumor development to 50 mm^3. After this MPB injection was initiated every alternate day in the tail vein with a total of 12 doses of treatment. Tumor volumes and body weight were measured every 3 days. The tumor size was calculated according to the formula: Tumor volume $(mm^3) = 0.52 \times L \times W^2$ where L is the length and W is the width. At the termination of the experiment on the 24th day, all animals were euthanized by cervical dislocation. At that time tumors and internal organs, such as the livers, spleens, lungs and kidney were excised from animals.

Histological and immuno-histochemistry studies

Tumor specimens were embedded into paraffin and the paraffin Sections (4-mm thick) were stained with hematoxylin and eosin or immunostained with p-p38MAPK (1:250) and PE tagged Ki67 (1:200). Images were captured using a confocal microscopy (Leica).

Statistical analysis

Values are shown as Mean ± S.E of mean except where otherwise indicated. Data were analyzed, and when appropriate, significance of the differences between mean values was determined by Student's t test. Results were considered significant at $p < 0.05$.

Results

Evaluation of anti tumorigenic effect of AMBI analogues led to the identification of the most active compound, mephebrindole

Breast cancer is the most frequent cancer in the female population. Although significant progress in the treatment of breast cancer has been achieved during past decades, it is still the principal cause of cancer death for females worldwide [25, 26]. Moreover most of the drugs like Tamoxifen, Cisplatin, Doxorubicin that are mainly used for breast cancer treatment, produce significant toxicity in the normal breast epithelial cells [27–30]. In the present study, we have used a cell-based small-molecule screening approach (the spectral details of all the compounds have been provided in Supplementary file 1) leading to the unbiased identification of a small molecule that selectively kills breast cancer cells over normal cells. As discussed earlier that DIM analogues have potent anticancer properties [15], we speculated that our synthetic analogues might also have some activity against human breast cancers. To selectively screen the potential anticancer agent(s) among the different synthetic DIM analogues, we initially evaluated these agents (Compounds 1–20) for their ability to reduce viability of MCF-7, HBL100, T47D breast cancer cells following 24-h exposure by MTT assay. Although the IC50 values of all DIM analogs were higher than 30 μM, some of the analogs in this series showed improved antitumor activity than DIM (Supplementary file 3). Among the few the most noteworthy of them was Compound 12, 3,3′-[(4-Methoxyphenyl) methylene]-bis-(5-bromo-1*H*-indole] (synthesis scheme provided in Supplementary file 2), and has been designated as mephebrindole (Fig. 1a). This compound exhibited IC50 values of 9.38, 10.2 and 9.3 μmol/L against MCF-7, HBL100 and T47D, respectively (Fig. 1b, left panel). This antitumor potency was two orders of magnitude higher than that of DIM (IC50, 75, 83 and 122 μM, respectively; (Fig. 1b, right panel). Moreover, assessment of the effects of this compound on nonmalignant cells revealed that normal breast epithelial cells (MCF10A) and Peripheral blood mononucleocytes (PBMC) exhibited a four to five fold lower sensitivity to MPB (IC50, 55, 48 μmol/L respectively) than the breast cancer cells (Fig. 1c). The major feasible issue in drug development process is elimination of maximum lead compounds at the higher stages of development as they fail in ADME (absorption, distribution, metabolism, and excretion), properties and it is not feasible to test each lead compound for ADME profiling with experimental methods. Thus prior ADME profiling, using theoretical tools which predict the ADME properties of unknown molecules is more cost effective prior evaluation. So we also evaluated the ADME profiling of MPB and interestingly observed that the ADME properties also identified MPB as the most effective in the group (Fig. 1d). These findings indeed prompted us to further delineate the detailed molecular mechanisms of MPB induced death of breast carcinoma cells.

MPB induced apoptosis in breast cancer cells is mediated through caspase activation as well as mitochondrial membrane potential (MMP) depolarization

Although our findings clearly showed that mephebrindole (MPB) possessed prominent anti carcinogenic properties

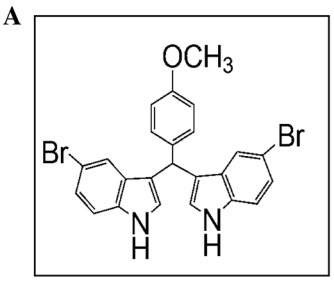

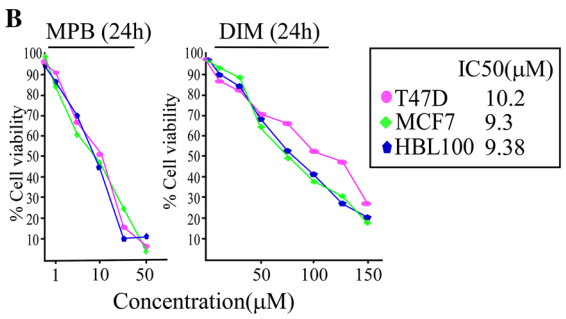

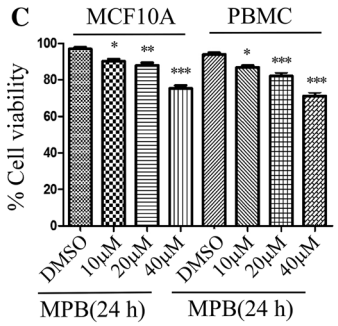

D **In silico predicted ADMET properties of Mephebrindole (MPB):**

QPlogHERG (predicted IC50)	- 6.507	Concern below -5
QPPCaco	2877.787	<25 poor, >500 great
QPlogBB	0.121	-3.0 to 1.2
QPPMDCK	10000	<25 poor, >500 great
QPlogKp	- 0.82	- 8.0 to -1.0
QPlogKhsa	1.552	-1.5 to 1.5
Percentage of human oral absorption	100	< 25% is poor
Formal charge	0	

QPlogHERG - Predicted IC50 value for HERG K+ channels. QPPCaco - Predicted apparent Caco-2 cell (model for gut-blood barrier) permeability in nm/s. QPlogBB - Predicted brain/blood partition coefficient. QPPMDCK - Predicted apparent MDCK cell (model for blood-brain barrier) permeability in nm/s. QPlogKp - Predicted skin permeability. QPlogKhsa C- Prediction of binding to human serum albumin. Range indicates the values desired for drug-like compound.

Fig. 1 The antiproliferative activity of mephebrindole on different breast cancer cell lines and ADME profiling **a** Chemical structure of 3,3′-[(4-Methoxyphenyl) methylene]-bis-(5-bromo-1*H*-indole), named as mephebrindole (MPB). **b** Effect of mephebrindole on the viability of breast cancer cell lines, MCF-7, HBL100 and T47D versus that of mother compound Di indolyl methane (DIM) has been represented graphically. Cells were treated with mephebrindole or DIM at the indicated concentrations in 10 % FBS—supplemented with DMEM in 96-well plates for 24 h, and cell viability was assessed by MTT assays. The IC 50 concentrations were determined using nonlinear regression analysis of Graph Pad Prism 6 software **c** Dose dependent antiproliferative effects of mephebrindole in on normal breast epithelial cell MCF-10A and peripheral blood mononucleocyte (PBMC) cells were represented graphically by *bar diagram*. The Trypan blue exclusion assay was used to determine the amount of MCF-10A and PBMC cell death in presence of MPB. MCF-7 cells were incubated with 10–40 μM of MPB for 24 h to assess their cellular growth and toxicity. **d** ADME (absorption, distribution, metabolism, and excretion) profiling, using theoretical tools which predict the ADME properties of unknown molecules MPB was tabulated

against breast cancer cells, however the mechanism involved are yet to be elucidated. To ascertain whether the effect of MPB on cell viability was caused by apoptotic cell death, MCF-7 and HBL-100, T47-D cells were treated with different concentrations of MPB for 24 h and apoptotic cell death was examined by annexin-V/FITC/PI double labeling (Fig. 2a). Annexin-VFITC/PI findings confirmed that most of anti-proliferative activity of MPB was mediated by

apoptosis. Alternation in mitochondrial membrane potential (MMP) is a common phenomenon in apoptotic cells. We therefore next examined whether MPB treatment produced any changes in the MMP of MCF-7 and HBL-100 cells. In response to MPB treatment breast cancer cells were found to demonstrate a dose dependent increase in the mitochondrial depolarization, reflected by decrease in percentage of polarized cells (Fig. 2b, upper panel). Subsequently, fluorescence images captured using the red and green filter of a fluorescence microscope clearly depicted the increase in green fluorescence level in 10 μM MPB treated MCF-7 cells in comparison to the untreated ones (Fig. 2b, lower panel). Furthermore, our western blot analysis of whole cell lysate from MPB treated MCF-7 and HBL100 cells showed a dose-dependent cleavage of caspase9, caspase3, caspase7 as well as PARP cleavage, a marker for caspase dependent apoptosis (Fig. 2c). Pro-apoptotic BAX and anti-apoptotic protein BCL-2 expression (Fig. 2d, upper panel) as well as their ratio (Fig. 2d, lower panel) was significantly altered following MPB treatment. Further, cytosolic Cytochrome *c* release was enhanced proportionally to MPB concentration (Fig. 2e). Prominent cytosolic localization of Cytochrome *c* was observed on10 μM MPB treatment in MCF-7 cells (Fig. 2f), which further signified the mitochondrial membrane depolarization. All the above findings suggested that MPB induced apoptosis through mitochondrial dependent apoptotic pathway. Though MPB was found to induce death in MCF-7 as well as HBL-100 cells, the further detailed mechanistic studies have been typically concentrated on the MCF-7 cells.

MPB induced apoptosis involves elevation of ER stress mediated through eIF2α phosphorylation and CHOP activation in MCF-7 cells

In order to delineate the molecular mechanism involved in MPB induced cell death we focused our investigations on the role of the ER stress pathway in the induction of apoptosis. Since UPR is an important genomic response to ER stress [31], the effects of MPB were examined in relation to UPR. Treatment of MCF-7 cells with MPB resulted in marked increase in the levels of UPR targets GRP78/Bip and CHOP in time dependent manners (Fig. 3a, lower panel). This also goes in line with the finding that increase in cell apoptotic rate induced by MPB in MCF-7 cells was dependent on the alterations of the above protein levels (Fig. 3a, upper panel). Furthermore, our observations revealed that phosphorylation of eIF2α appeared at 9 and 12 h, but was not sustained beyond 24 h. However on the other hand the induction of the downstream transcription factor ATF4 by MPB gradually increased regardless of the phosphorylation status of eIF2α (Fig. 3a, lower panel). Our findings from Western blot analysis (Fig. 3b, upper panel) and immuno-cytochemistry (Fig. 3b, lower right panel) also revealed that ATF4 expression was substantially elevated in both the cytoplasm and the nucleus on treatment with MPB. qRT PCR data also validated our findings that CHOP expression was elevated in transcriptional level also due to MPB treatment in MCF-7 cells at different time point (lower left panel).In contrast, MPB had little or no effect on expression of other UPR pathway regulated proteins like ATF6 and IREIα as evident from both western blot and RT PCR analysis (Fig. 3c, left and middle panel). However, spliced XBP1 mRNA was hardly visible after 24 h of MPB treatment, but the total XBP1 mRNA expression remain unchanged under this condition in MCF-7 cells (Fig. 3c, right panel). Thus from preceding findings we hypothesized that a different apoptosis response was induced, at least in part through the differential activation of the transcription factor ATF4 and CHOP through GRP78/PeIF2α pathway. Recent studies indicate that eIF2α phosphorylation is required for cell survival, and inhibition of eIF2α phosphorylation promoted cell death [32, 33]. Salubrinal selectively blocked de-phosphorylation of eIF2α and protected cells against ER stress mediated apoptosis [34, 35]. We next examined whether salubrinal could protect MCF-7 cells against MPB induced apoptosis. Salubrinal at a dose of 10 μM had no effect on MCF-7 cells apoptosis, despite inducing eIF2α phosphorylation (Fig. 3d, lower panel). Unexpectedly co-administration of salubrinal and MPB significantly enhanced MPB mediated apoptosis (Fig. 3d, upper panel). Such findings are consistent with the above results that MPB mediated MCF-7 cells apoptosis depends on phosphorylation status of eIF2α. CHOP, a C/EBP family transcription factor activated protein is a major component of the ER stress-mediated apoptosis pathway. We thus investigated the role of CHOP in MPB-induced ER stress mediated cell death. MPB treatment significantly reduced cell viability, as determined from Annexin V-PI staining (Fig. 3e, upper panel). Whereas, CHOP siRNA, significantly inhibited MPB-induced PARP cleavage (Fig. 3e, middle panel) as well as the BAX/BCL-2 ratio (Fig. 3e, lower panel). MPB -induced apoptosis, detected by Annexin V-PI staining, was also suppressed by CHOP siRNA (Fig. 3e, upper panel). These results clearly indicated that ER stress is involved in MPB induced apoptotic cell death and activation of eIF2α/ATF4/CHOP mediated UPR signaling is solely involved in this apoptosis induction.

Calcium acts as an upstream regulator of MPB induced ER stress activation

After identifying ER stress induction and UPR gene expression, we tried to clarify the upstream signaling cascades underlying the action of MPB in MCF-7 cells and

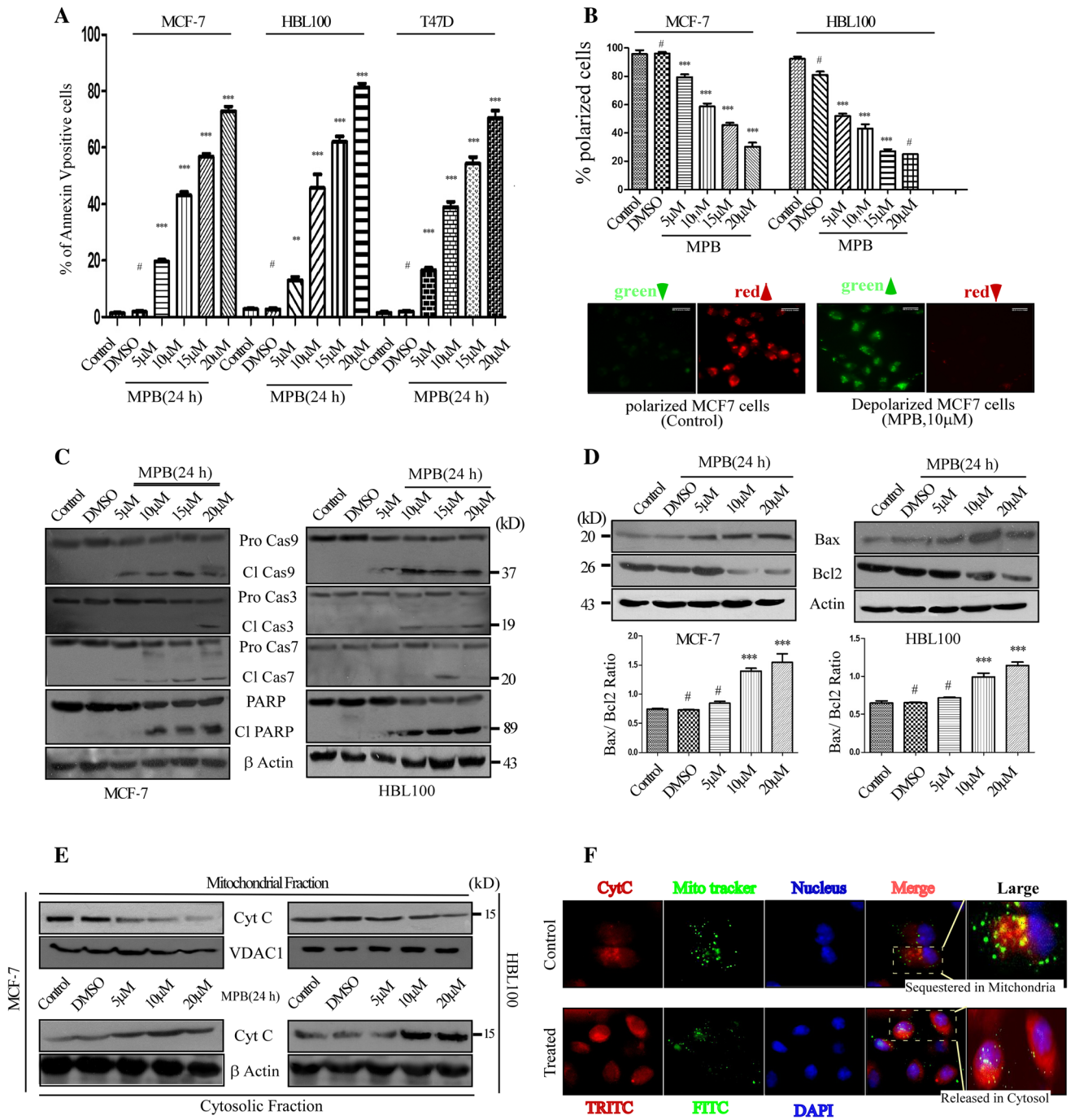

Fig. 2 The antiproliferative activity of mephebrindole on different breast cancer cell lines is mediated by apoptosis through mitochondrial dependent pathway. **a** MCF-7, HBL100, T47D cells were treated with different doses of mephebrindole for 24 h. Apoptosis was determined by AnnexinV-FITC/PI FACs analysis. The *bar diagrams* represents the summary of mean percentage ± SD of apoptotic cells (late and early apoptotic) of three independent experiments. **b** Mephebrindole collapsed the mitochondrial membrane potential in MCF-7 a dose dependent manner. Cells were treated with or without mephebrindole for 24 h and then stained with JC1 dye. FACS analysis was done to calculate % of polarized cells (*upper panel*). Subsequently, the fluorescence images were captured using the red and green filter of a fluorescence microscope (*lower panel*). **c** Western blot analysis depicting the changes in the expression level of cleaved PARP, Caspase9, Caspase7, Caspase3 at different concentration of MPB treatment in MCF-7 and HBL100 cell lines. β-actin was used as internal loading control. **d** MPB altered the expression of Bax, BCL-2 (*upper panel*), and also the ratio (*lower panel*) in the both cell lines at different doses. **e** The cytosolic and mitochondrial expression level of Cytochrome *c*, treated with mephebrindole at different concentration of two cell lines was determined from Western blot analysis. We used VDAC1 and beta actin as a loading control for mitochondrial and cytoplasmic fraction respectively. **f** Cytochrome *c* release was confirmed by double immunostaining with anti cytochrome *c* antibody and mito-tracker in MCF-7 cells

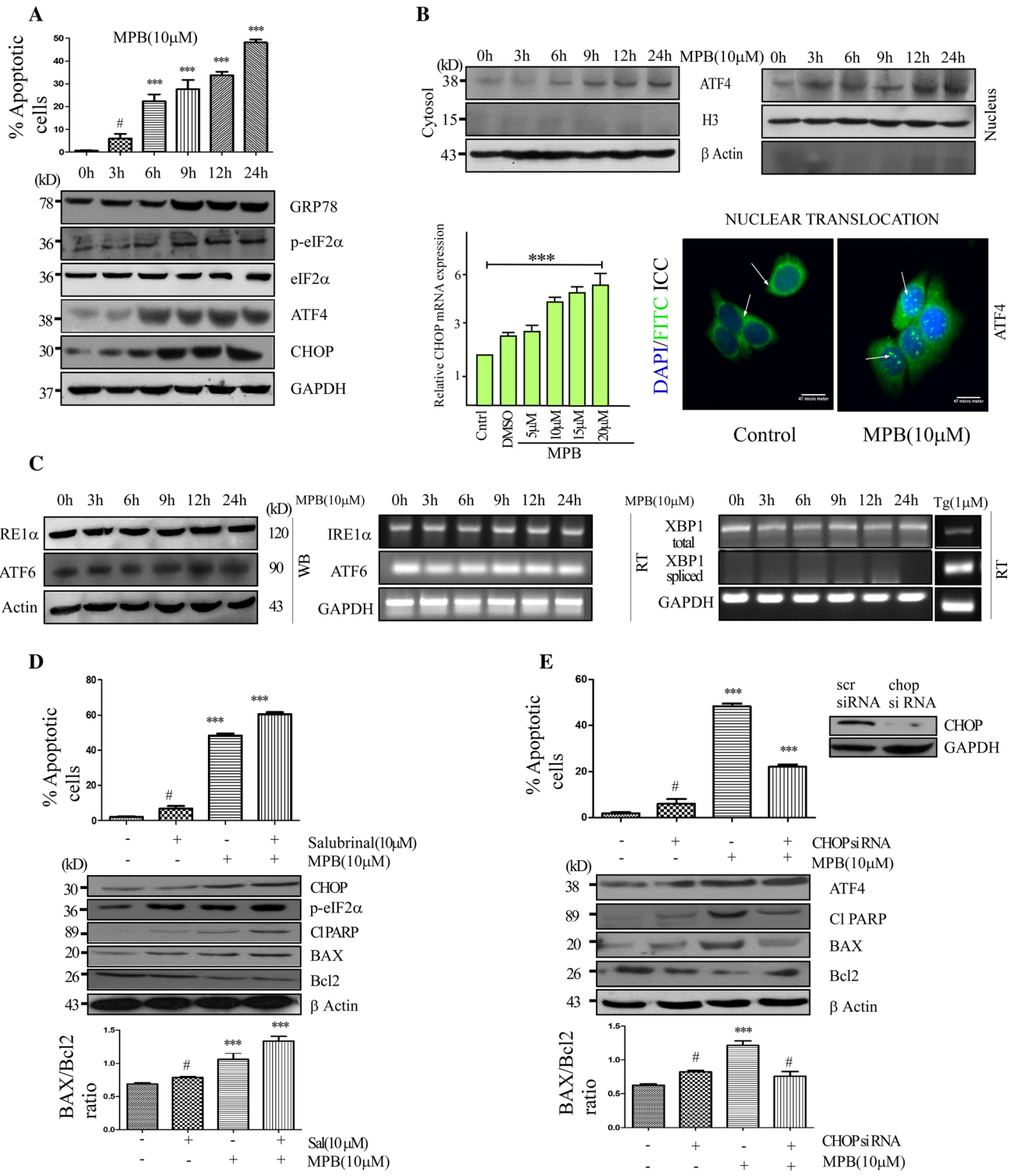
A
MPB(10μM)
% Apoptotic cells
0h 3h 6h 9h 12h 24h
(kD)
GRP78
p-eIF2α
eIF2α
ATF4
CHOP
GAPDH
B
0h 3h 6h 9h 12h 24h MPB(10μM) 0h 3h 6h 9h 12h 24h
Cytosol
Nucleus
ATF4
H3
β Actin
Relative CHOP mRNA expression
Cntrl
DMSO
5μM
10μM
15μM
20μM
MPB
NUCLEAR TRANSLOCATION
DAPI/FITC ICC
ATF4
Control
MPB(10μM)
C
IRE1α
ATF6
β Actin
WB
RT
XBP1 total
XBP1 spliced
GAPDH
Tg(1μM)
D
Salubrinal(10μM)
MPB(10μM)
CHOP
p-eIF2α
ClPARP
BAX
Bcl2
β Actin
BAX/Bcl2 ratio
Sal(10μM)
E
scr siRNA
chop si RNA
CHOPsiRNA
Cl PARP

◀**Fig. 3** ER stress mediated CHOP induction was the main determinant of MPB induced MCF-7 cells apoptosis. **a** Mephebrindole induced the ER stress related Grp78/eIF2α/ATF4 pathway, and downstream CHOP activation to induce apoptotic cell death. MCF-7 cells were treated with 10 μM MPB, collected at various intervals and lysed. Lysate were subjected to Western blot assay (*lower panel*). In addition, cells were stained with Annexin V-PI (*upper panel*), and % of apoptotic cells were measured in FACS. **b** Cytoplasmic (*upper left*) and Nuclear fractions (*upper right*) were isolated at indicated times, and ATF4 was examined by Western blot analysis. Graphical representation of the changes in the mRNA expression of CHOP in the aforementioned sets (*Lower left panel*) clearly showed transcriptional upregulation of CHOP by MPB treatment. Fluorescence staining against ATF4 clearly showed the increase of ATF4 level in nucleus of MPB treated MCF-7 cell (*lower right panel*). **c** MCF-7 cells were incubated with 10 μM MPB for various time intervals and expression levels of the UPR related proteins, IRE1α, ATF6 were determined by Western blot analysis (*left panel*) and RT-PCR (*middle panel*) analysis. RT-PCR analysis determining the changes in total and spliced XBP 1 expression levels for different time intervals on treatment with 10 μM MPB in MCF-7 cells (*right panel*) for positive control we used Thapsigargin as an ER stress inducer. **d** MCF-7 cells were treated with 10 μM salubrinal or 10 μM MPB, or both for 24 h and % apoptotic cell death (*upper panel*) was determined using Annexin V-FITC/PI analysis. Simultaneously the expression of CHOP, peIF2α and different apoptosis related marker proteins were determined by Western blotting (*middle panel*). The change of BAX/BCL-2 ratio was plotted (*lower panel*) at 24 h treatment of salubrinol, MPB or salubrinal + MPB in MCF-7 cells. **e** MCF-7 cells were transfected with si RNA CHOP, incubated with MPB for 24 h and then expression levels of Cl PARP, BAX, BCL-2 and ATF4 was were determined by immunoblotting (*middle panel*) Percent apoptotic cells were also quantified using flow cytometric analysis (*upper panel*). Changes in BAX/BCL-2 ratio was also indicated in *lower panel* in same aforementioned condition (*inset*) following knocking down of CHOP using CHOP siRNA. The blots are representative of at least three separate experiments and β-actin was used as control. The statistical analysis of graphs was presented as the mean ± SD. $^{*}p < 0.05$ compared with MPB treated cells

henceforth checked the changes in cytosolic calcium levels of the MCF-7 cells on treatment with MPB. Interestingly, our findings revealed that the treatment of MCF-7 cells with MPB resulted in a gradual rise in cytosolic calcium level in a time dependent manner. Fluo 3-AM loaded cells were exposed to MPB (10 μM) for different time periods and subjected to live cell fluorescence imaging. The results presented in Fig. 4a clearly highlighted a gradual increase in $[Ca^{2+}]_c$ in MCF-7 cells in time dependent fashion. Using microplate reader with the Fluo 3-AM, the increase in $[Ca^{2+}]_c$ was estimated to be close to 40 % after 3 h (Fig. 4b, left panel) which ultimately resulted in a situation of cytosolic calcium overload in MCF-7 cells (Fig. 4b, right panel). Furthermore, since $[Ca^{2+}]_{er}$ release can be both a cause and a consequence of ER stress we first determined whether the response of MCF-7 cells to TG [TG irreversibly inhibits (sarco) endoplasmic reticulum Ca^{2+} ATPase (SERCA) and depletes ER calcium stores] could be altered by MPB. To this end, vehicle treated control cells or cells pretreated with MPB for 180 min were stimulated with TG (1 μM) after removal of extracellular calcium with 2 mM EGTA (Fig. 4c) and $[Ca^{2+}]_{cyt}$ was measured. The results significantly displayed that the TG-driven rise in the $[Ca^{2+}]_{cyt}$ was attenuated when cells were pre-treated with MPB. Indeed, Fig. 4c distinctly highlighted that the response to TG was decreased by approximately 46 % (under MPB treated conditions). These findings therefore suggested that MPB slowly depleted calcium from the ER resulting in the generation of ER stress. Hence we raised the question whether this calcium alteration was enough to produce ER stress mediated CHOP activation and apoptosis induction in MPB treated MCF-7 cells. To address this question we used intracellular calcium chelator BAPTA-AM with MPB. Interestingly our results showed that co-administration of BAPTA-AM with MPB could not fully attenuate the apoptotic effect of MPB (Fig. 4d, upper panel) whereas it effectively lowered the expression of GRP78 and moderately changed the expression of downstream UPR effectors of MPB treated cells (Fig. 4d, lower panel) thereby suggesting the involvement of any other mediator along with calcium to regulate the ER stress pathway. These findings thereby inclined us to further investigate another alternative upstream modulator that also modulates eIF2α/ATF4/CHOP signaling cascade in the presence of MPB.

Activation of p38MAPK facilitated MPB induced apoptosis in MCF-7 cells

As MAPK has known roles in various stress signal transduction pathways [36, 37], the MAPK inhibitors SP600125 (JNK), SB203580 (p38MAPK), UO126 (ERK) were combined with MPB to examine the apoptotic level as well as the ATF4 expression. We observed that the addition of SB203580 to the MCF-7 cell cultures in the presence of MPB partially attenuated the apoptotic effect of the former (Fig. 5a, upper panel) as well as altered the expression of ATF4, (Fig. 5a, lower panel), but the other inhibitors in combination with MPB had no effect on ATF4 expression as well as apoptotic cell death. The activity label of these different MAPK inhibitors at these used concentrations were shown in Fig. 5b. This finding clearly suggested the involvement of p38MAPK in ER stress related cell apoptosis. Figure 5c showed that the induction of p38MAPK activity by MPB occurs in time (upper panel)-and dose dependent (lower panel) manners in MCF-7 cells. To gain further insight into the mechanisms by which p38 regulates apoptosis we explored the interaction between p38 and the GRP78/eIF2α/ATF4 pathway. Figure 5a already highlighted that inhibition of p38 hampered the expression of p-eIF2α and ATF4 significantly whereas upstream GRP78 was not affected. GRP78 silencing of MCF-7 cells via

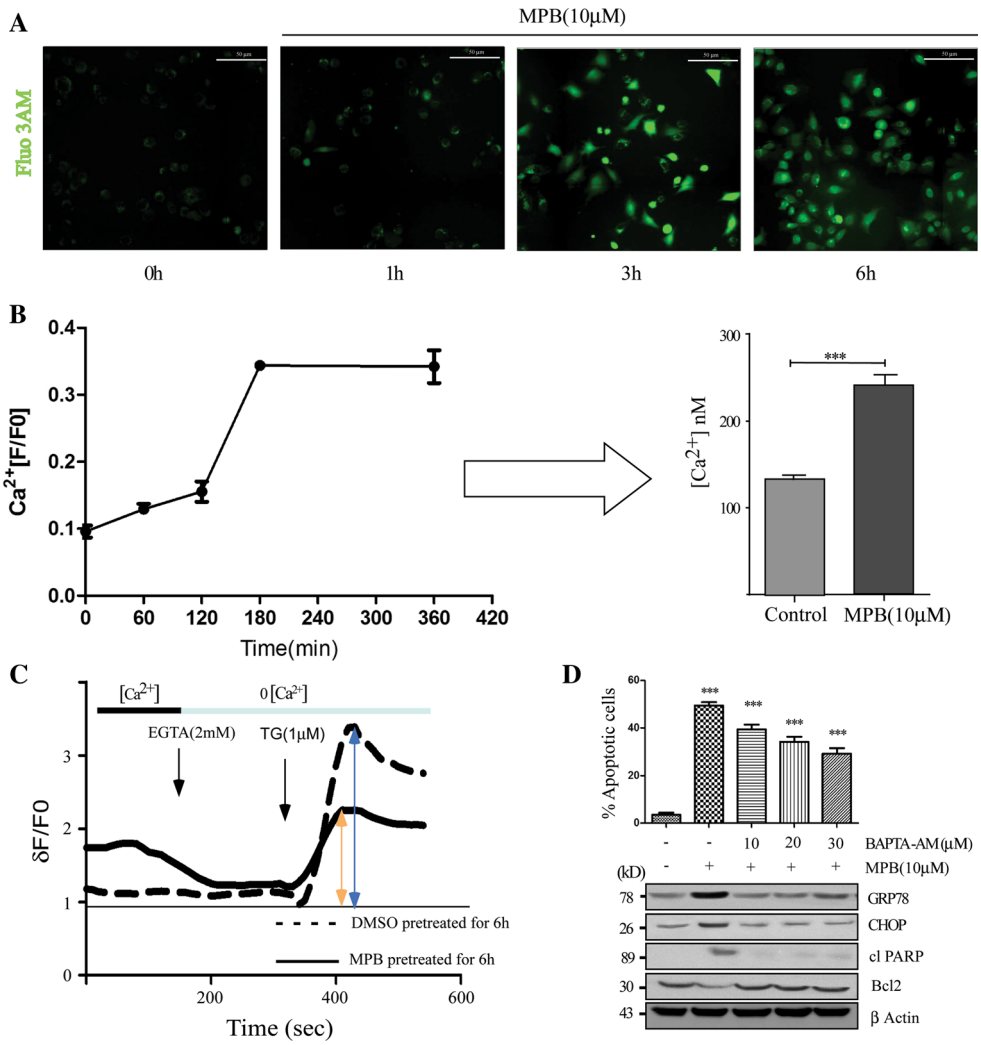

Fig. 4 Internal store depletion by MPB resulted in cytosolic calcium hike and death of MCF-7 cells. **a** Cells were cultured in the presence of mephebrindole at indicated time periods. One hour prior to the analysis, Fluo 3AM was added to the final concentration of 10 μM MPB and the images were acquired using a fluorescence microscope. **b** Intracellular calcium level was quantified using a fluorescence microplate reader as described under materials and methods section. Results are expressed graphically as $\delta F/F_0$ (*left panel*). Concentration of intracellular calcium was measured in living cells with and without exposure to mephebrindole for 3 h using the calcium indicator dye, fluo 3AM as described under materials and methods section. Results are represented as mean ± SEM. (*right panel*) **c** Cytosolic calcium was measured using fluo3-AM as fluorescence dye. The release of $[Ca^{2+}]_{er}$ by TG was compared in mephebrindole-treated cells versus control MCF-7 cells (n = 4). Extracellular calcium was depleted for 3 min before addition of TG (1 μM) in order to avoid capacitative calcium influx. TG-mediated $[Ca^{2+}]_c$ was increased and $\delta F/F_0$ was plotted graphically. **d** MCF-7 cells were treated with different concentration of intracellular calcium chelator BAPTA-AM in presence or absence of MPB. % of apoptotic cells were quantified by FACS (*upper panel*). Subsequently expression level of CHOP and apoptotic marker proteins were determined by Western blotting (*lower panel*). Results are expressed as percentage of control and represented as mean ± SEM (n = 3). *Statistically different ($p < 0.05$) from the condition without mephebrindole

siRNA (Fig. 5d) or treatment with BAPTA AM (Fig. 5e) left the phosphorylation status of p38 unaltered in the presence of MPB. Furthermore we also checked the effects of eIF2α on p38 activity. Salubrinal, a cell permeable eIf2α agonist effectively activated eIF2α in MCF-7 cells. However, salubrinal treatment exerted limited effects on p38 phosphorylation but ATF4 expression was highly increased (Fig. 5f). These result demonstrated that p38 acts between Grp78 and eIF2α to promote signal transduction to ATF4.

MPB mediated ER stress generation and p38 activation potentiated the recruitment ATF4 to the CHOP promoter

To elucidate the role of ATF4 expression in apoptosis induction and considering our previous results, we next investigated the link between ATF4 and CHOP gene transcription in response to MPB. The ATF/CREB family consists of transcription factors that function by binding to

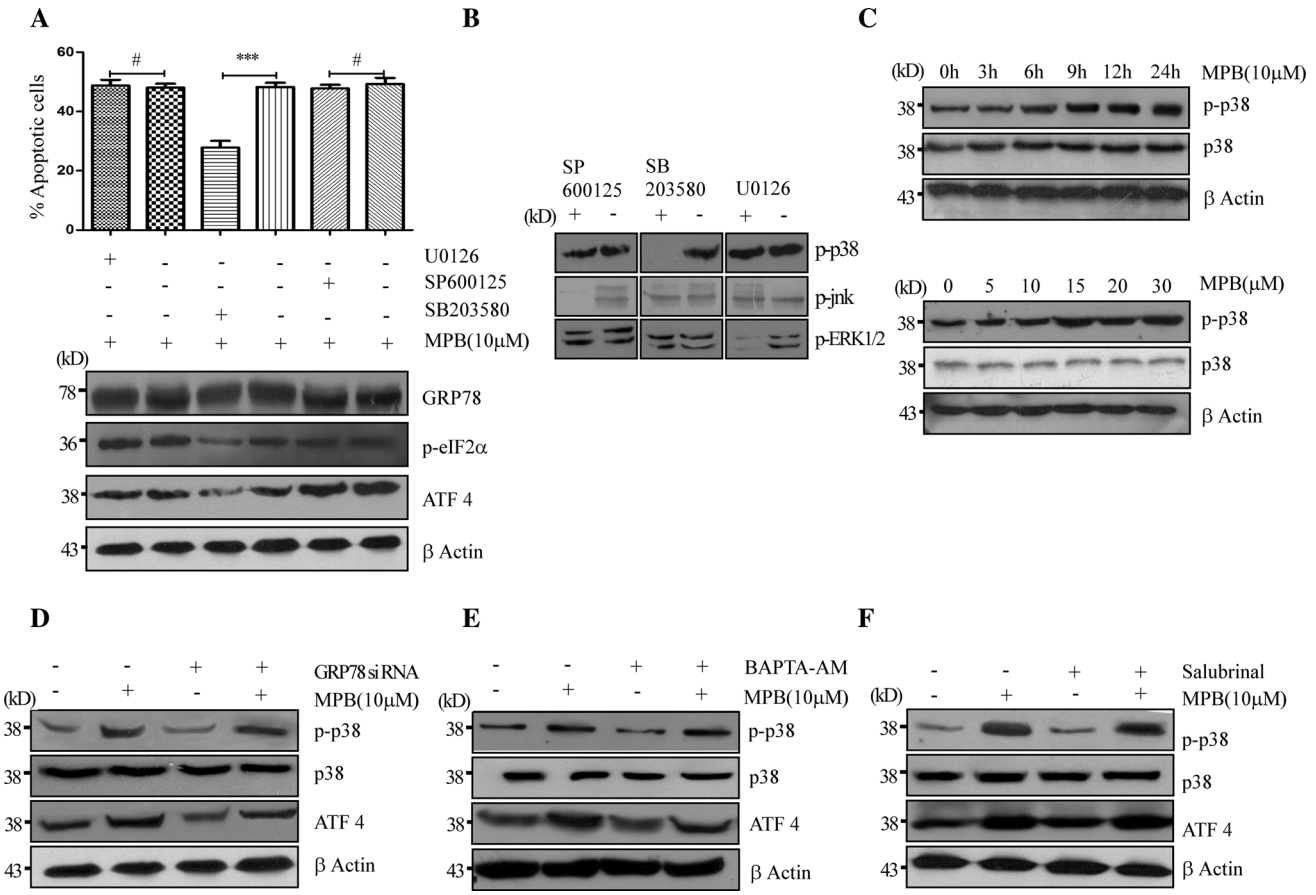

Fig. 5 p38MAPK was involved in MPB induced ATF4 induction in MCF-7 cells. **a** MCF-7 cells were pretreated with U0126 (10 μM) or SP600125 (10 μM), SB 203580 (10 μM) for 1 h and then stimulated with MPB (10 μM) for 24 h. Percent of apoptotic cells and protein levels of Grp78/eIF2α/ATF4 pathway were measured by FACS and immunoblot analysis respectively. **b** The effect of different MAPK inhibitors on phosphorylation status of different MAPKs at their used concentration were shown by Western blots. **c** MPB activates p38MAPK in a time and concentration dependent manner. MCF-7 cells were treated with 10 μM MPB for various time periods (*upper panel*) or with the indicated concentration of MPB for 24 h (*lower panel*), and phospho p38 and p38 levels were determined by immunoblotting. **d** Following GRP78 inhibition using GRP78 siRNA and subsequent MPB exposure, the expression of phospho-p38, p38 and ATF4 were examined by western blotting. **e**–**f** Cells were treated with 10 μM BAPTA-AM (25 μM) (**e**) or salubrinal (**f**) alone or in combination with MPB and the aforementioned proteins were detected by Western blot analysis

the cAMP-responsive elements (cre) palindromic octanucleotide [9, 38]. Previous reports [13] already depicted the importance of the another C/EBP-ATF composite site for CHOP regulation during ER stress. Henceforth, computational analysis of the CHOP promoter revealed the existence of one C/EBP-ATF composite site at −330 region (Chop1), where as cre like elements at nt-750 (Chop2) region (Fig. 6a). Subsequent our ChIP assays confirmed an enrichment of ATF4 on both the site but greater extent in Chop1 site (Fig. 6b). Moreover it is noteworthy that the amount of enriched ATF4 on the CHOP promoter increased following the addition of MPB to MCF-7 cells whereas SB203580 or BAPTA-AM co treatment markedly inhibited the recruitment because of the simultaneous inhibition of p38MAPK and cytosolic calcium hike in MCF-7 cells (Fig. 6c). Therefore the aforesaid data suggested that MPB induced cytosolic calcium hike and p38 activation both were equally responsible for ATF4 recruitment in CHOP promoter and its induction to produce higher percent of cell death in MCF-7 cells.

MPB induced CHOP mediated cell death through development of oxidative stress

Increased ER stress would require increased disulphide bond formation where electrons are shuttled through protein disulphide isomerase and O_2 to generate H_2O_2 [39]. Dichloro fluorescein staining detected increased ROS level following MPB treatment (Fig. 7a, b). Several previous reports [40] already showed that CHOP over expression caused ROS generation in different cells line. Keeping this in our mind we speculated the role of CHOP in MPB

induced ROS production. Western blot analysis as well as RT-PCR data showed that increasing concentration of NAC with MPB treatment did not change the expression level of CHOP (Fig. 7c). But when we knocked down CHOP in MCF-7 cells in the presence and absence of MPB and measured the ROS level after 24 h, we observed that CHOP silencing reduced ROS generation and significantly increased polarized cell number in presence of MPB. Similar observation was also obtained on treatment with antioxidant, NAC in the presence of MPB thereby indicating that ROS generation mediated mitochondrial death cascade activation acted downstream of CHOP activation (Fig. 7d, e). All these findings thus cumulatively indicated that MPB couples the ER stress and p38MAPK to facilitate ATF4 recruitment to the CHOP promoter which promotes ROS generation and causes cell death via depolarization of mitochondrial membrane potential and caspase activation.

Re-validation of in vitro results in tumor allograft bearing mice models

EAC derived from breast adenocarcinoma is an aggressive and rapidly growing carcinoma commonly used for the evaluation of the effect of novel small molecules on tumor progression. In order to further establish the importance of MPB as an anti-carcinogenic agent we injected the Swiss Albino mice with EAC and treated them with different doses of MPB. After fourth day of EAC injection a small size tumor was found to appear. The animals were then randomized into three groups of ten mice each (Untreated, 10 mg/Kg and 20 mg/Kg MPB treatment) and subjected to MPB treatment every alternate day and a total of 12 doses were applied. It has been observed that MPB was most prominently effective at a dose of 20 mg/Kg body weight. The gross appearance of thigh tissue containing tumor and also the excised tumor of untreated control mice (Fig. 8a, upper panel) and 10 mg/Kg (Fig. 8a, middle panel) 20 mg/Kg (Fig. 8a, lower panel) MPB treated mice showed significant morphological changes. The tumor sections were also analyzed histologically (Fig. 8b, first panel), followed by Ki67 staining which showed a decline in proliferation on treatment with MPB (Fig. 8b, second panel). This was followed by H&E staining of the excised liver (Fig. 8b, third panel), lungs (Fig. 8b, fourth panel), kidney (Fig. 8b, fifth panel), spleen (Fig. 8b, sixth panel) which also showed distinct morphological changes on MPB treatment.

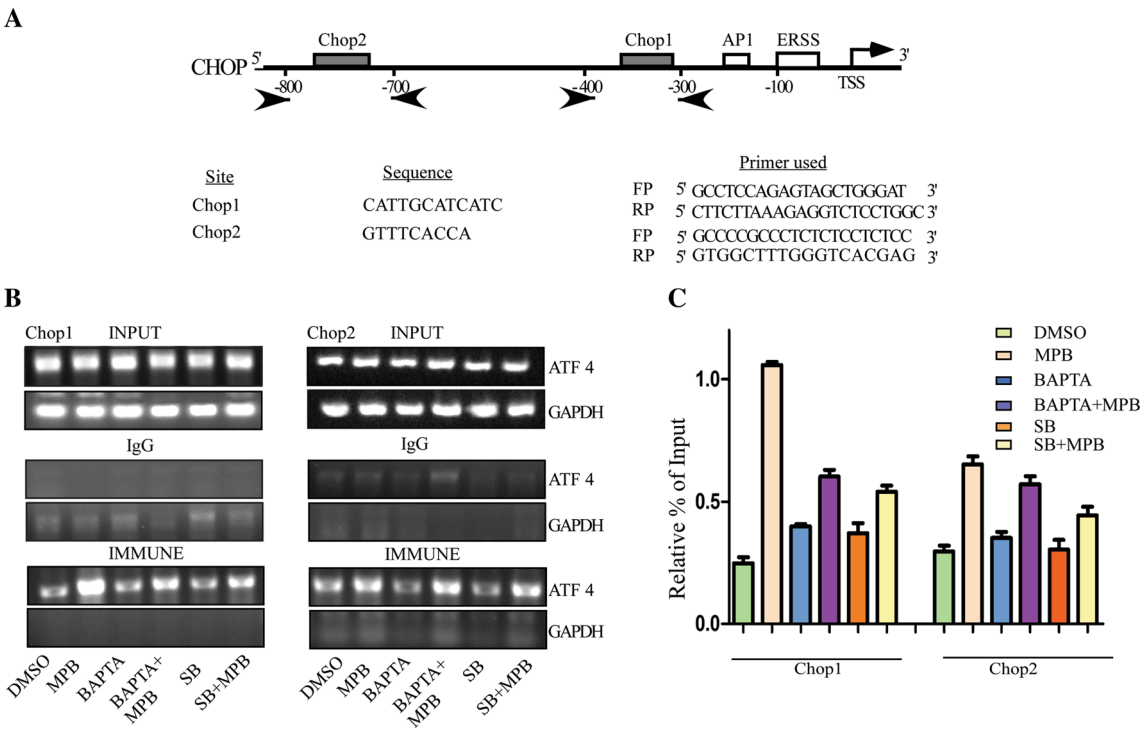

Fig. 6 MPB potentiated the reqruitment of ATF4 into the CHOP promoter. **a** A schematic diagram showing the location of the sequences detected by reverse transcriptase PCR analysis following CHIP experiment. **b** Chip assay in MCF-7 cells in the presence or absence of MPB and different modulators (BAPTA AM and SB 203580) demonstrated the recruitment of ATF4 in two different Chop1 (*left panel*) and Chop2 (*right panel*) CHOP promoter sites. GAPDH used as a control. **c** Relative quantity of CHOP gene promoter occupied by ATF4 in MCF-7 cells under different conditions. Cells were co-treated with SB203580, BAPTA-AM or MPB, and a Chip assay was performed using an anti- ATF4 antibody and negative control IgG. The precipitated DNA was then assessed using reverse transcriptase PCR. The statistical graphs are presented as the mean ± SD of three independent experiments.*$p < 0.05$ compared with MPB treated cells

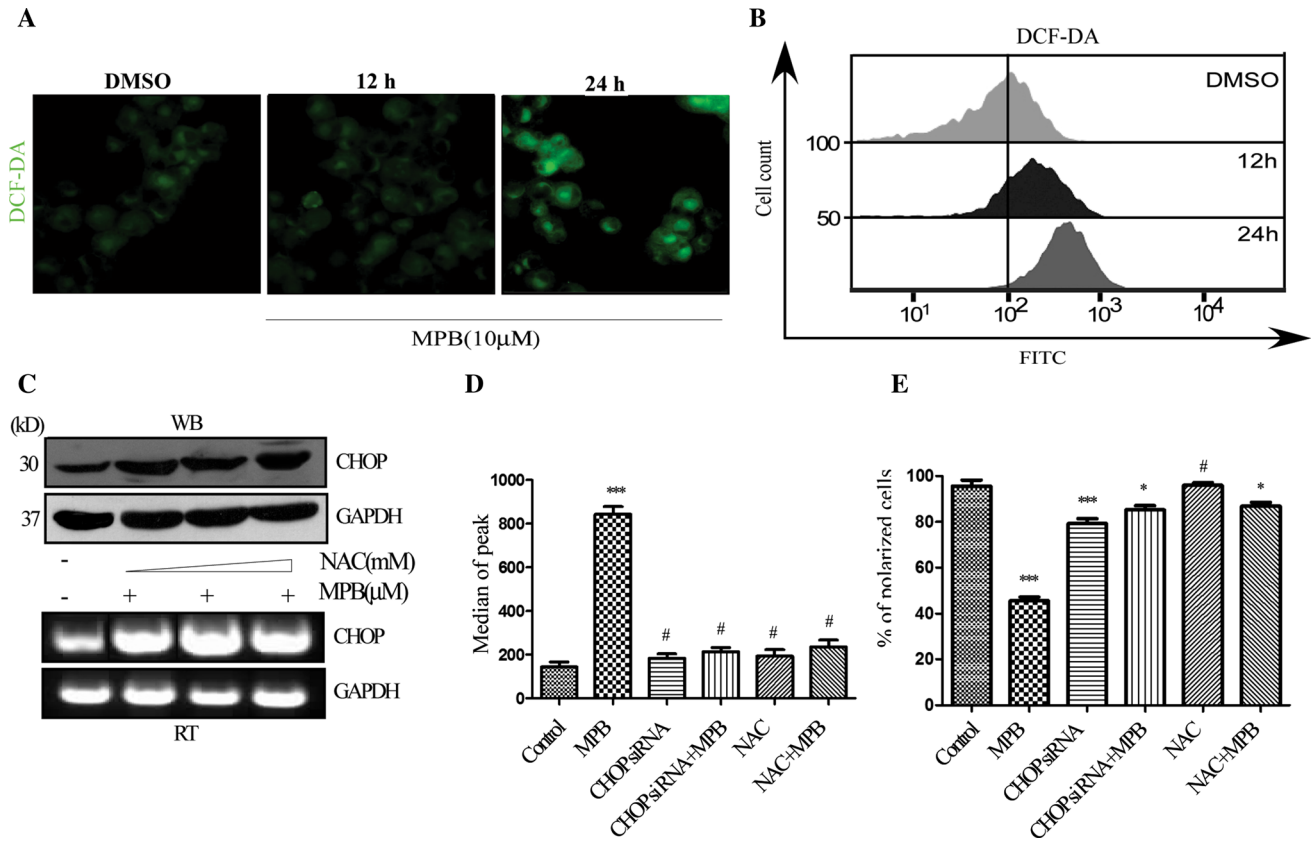

Fig. 7 CHOP mediated ROS generation caused mitochondrial membrane depolarization in MPB treated MCF-7 cells. **a**–**b** MCF-7 cells were incubated with 10 μM MPB for the indicated time periods, followed by treatment with DCFH-DA for 30 min. Formation of ROS was measured by fluorescence microscope (**a**) and flow cytometry. **b** DCF fluorescence was plotted as the mean ± SEM of at least three experiments. **c** Western blot and RT-PCR analysis of CHOP treated with MPB and increasing concentration of NAC. GAPDH was used as loading control. **d** Graphical representation of the percentage of ROS production represented as median of peak in MCF-7 cells treated with MPB alone or in the presence CHOP siRNA or in the presence of NAC. **e** Graphical representation of the percentage of polarized cells obtained from flow cytometry in MCF-7 cells treated with MPB alone or in the presence of CHOP siRNA or in the presence of NAC

Absolute volume and gross weight loss of thigh tissue containing tumor of untreated and MPB treated animals (Fig. 8c, d) further confirmed the effect of MPB on regression of tumor. IHC was then performed using phospho p38 antibody and prominent up-regulation in the phospho p38 levels was observed in the MPB treated groups (Fig. 8e, upper middle and lower panel).The Western blot analysis also revealed activation of p38 levels as well as activation of the BAX, cleaved PARP and ER stress related protein (GRP78, ATF4 and CHOP) which is also in line with the in vitro findings (Fig. 8f). Further studies also showed that the tumor burden resulted in a significant elevation in the serum gamma glutamyl transferase, alkaline phosphatase, urea and creatinine levels (Supplementary file 5). However, MPB provided a complete safeguard to the liver and kidney restoring to the normal level.

Thus cumulatively our findings critically establish MPB acts as an effective anti-cancer agent (Fig. 9) which may be a suitable candidate for anti-breast cancer drug development in future.

Discussion

Most available breast cancer therapies like tamoxifen are not always successful, either because the tumors do not respond to the treatment at all, or they develop drug resistance over time. Thus there is a continuous need to develop alternative effective therapeutic treatment. The prospect of dietary indole derivatives as anti-cancer therapeutics is thus a very promising area of research. In the present study, we focused on an AMBI derivative, mephebrindole and its effect on breast cancer cells highlighting the internal calcium store depletion and p38 activation simultaneously through CHOP mediated ROS generation.

It has been previously acknowledged that intracellular calcium [$(Ca^{2+})_i$] is a second messenger and signal transducer in both excitable and non-excitable cells and is critically involved in physio- and pathological processes [41]. Under normal conditions, the intracellular calcium concentration is maintained at 10–100 nM, but sustained

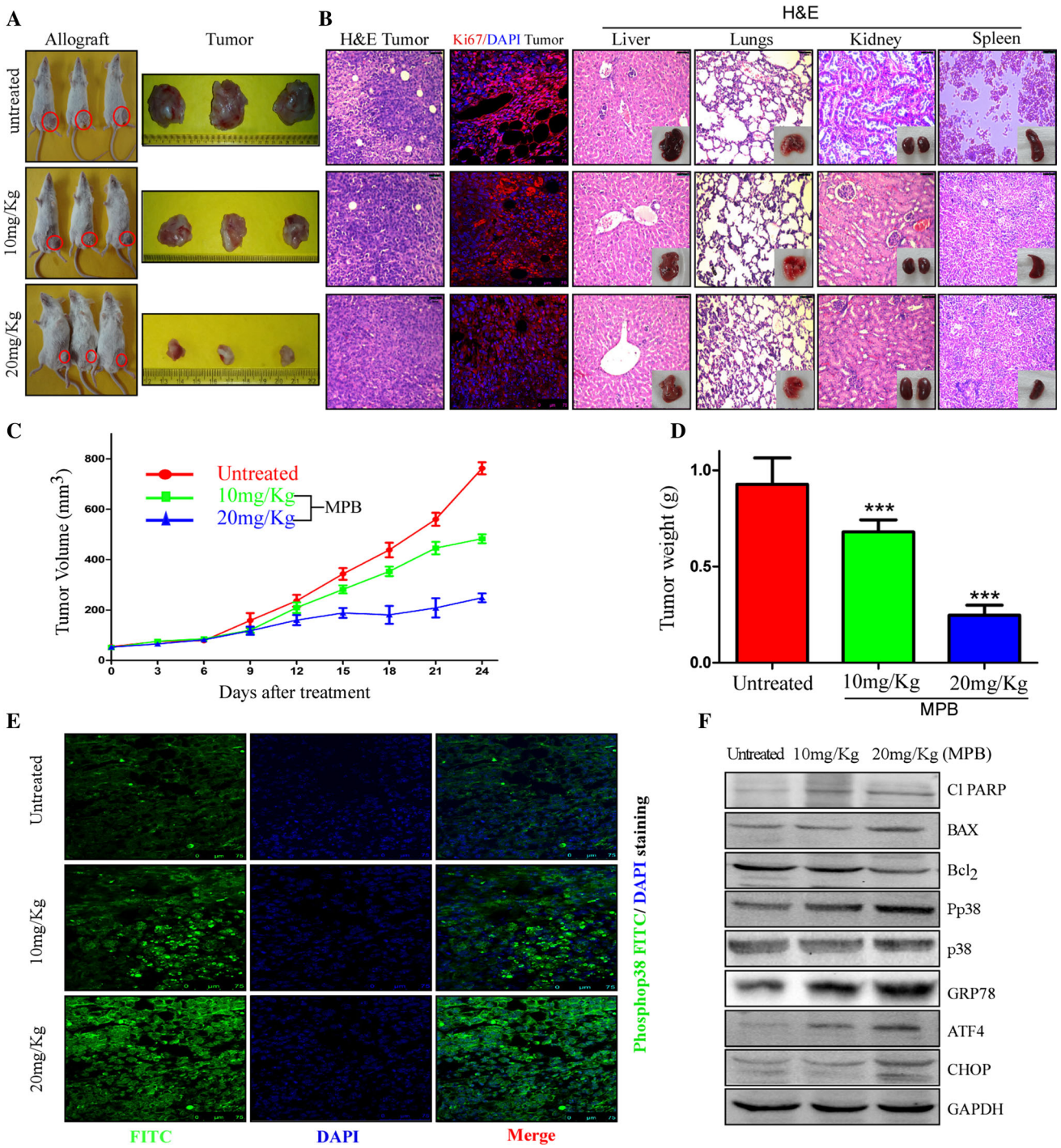

Fig. 8 MPB regressed EAC growth in Swiss albino allograft mice models. **a** Representative images of EAC derived Allograft untreated (*upper panel*) and treated with two different doses of MPB, 10 mg/Kg body weight (*middle panel*), 20 mg/Kg body weight (*lower panel*). **b** H&E staining of paraffin-embedded sections of the liver, lungs, spleen and kidney (20×). MPB did not cause obvious pathologic abnormalities in normal tissues. **c** Tumor volume curve of mice from untreated, 10 and 20 mg/Kg of MPB treatment. *Bars* represent standard deviation of the volume of tumors at each time point. **d** Tumor weight was evaluated on the day of sacrifice in all the above mentioned set. Data presented as mean ± SEM. **e** IHC analysis of phospho p38MAPK in the tumor tissues obtained from the above mentioned sets. **f** Expression and activation of cleaved PARP, Bax, BCL-2, GRP78, ATF4, CHOP and phosphop38 in tumor tissue lysates isolated from untreated and treated groups as examined by immunoblotting

Ca^{2+} release from calcium stores, Ca^{2+} influx through receptor- or voltage-dependent calcium channels or blockage of re-uptake can perturb $[Ca^{2+}]_i$ homeostasis. A modulation of $[Ca^{2+}]_i$ is thus an important factor in the activation of programmed cell death [42, 43]. Our results significantly illustrated a prominent increase in cytosolic calcium in MCF-7 cells when treated with MPB. This hike in cytosolic calcium level may have occurred due to either internal store depletion or increase in extracellular calcium entry through activation of different plasma membrane calcium channels. But in our experimental set up, internal store depletion was found to be the major causative agent behind this calcium overload.

It is well established that internal store depletion causes disturbance in the folding capacity of the endoplasmic reticulum (ER), leading to a cellular stress condition known as ER stress. Studies over the past decade have linked the Grp78/eIF2α/ATF4 UPR branch to ER stress related apoptosis in various disease [2]. Recent report demonstrated that ATF4 which is a substrate of eIF2α, increased the transcription of essential apoptotic genes [3]. In accordance with that we determined the binding of ATF4 at C/EBP-ATF composite site or CRE-like elements in the CHOP promoter, which is involved in anti-apoptotic protein, BCL-2 down regulation, a hallmark of ER stress mediated apoptosis. Our observations revealed transient activation of eIF2α during exposure of MCF-7 cells to MPB, indicating chronic ER stress induction leading to cellular adaptation and also hinted us to the involvement of an alternative pathway in the activation of ATF4 in MCF-7 cells.

The mitogen-activated protein kinases (MAPKs) mainly are involved in the development and progression of cancer and are also associated with ER stress. ERK1/2 is activated by growth factors, while p38 and JNK are mainly activated by cellular stresses. By using specific inhibitors in presence of MPB we nullified the involvement of ERK or JNK in MPB induced MCF-7 cells apoptosis. It has been reported that the p38MAPK pathway is required for the induction of the ER stress marker protein GRP78, as well as eIF2α activation. In fact our findings also highlighted enhanced phosphorylation of p38 by MPB leading to eIF2α phosphorylation. Furthermore, administration of MPB with a p38MAPK inhibitor also confirmed that p38 activation contributed to ER stress development in MCF-7 cells in presence of MPB. Thus our observations could be culminated that MPB induced eIF2α phosphorylation favored ATF4 mediated prolonged activation of CHOP which thereby triggered the mitochondrial apoptotic cascade to induce substantial death of MCF-7 cells.

In the present study we have identified increased mitochondrial depolarization as one of the mechanisms by which CHOP mediated cell death in response to MPB occurred. Although CHOP is known to be a pivotal player in ER stress mediated death, CHOP binding to genes known to function in cell death, including BCL-2 [40], Bax [38, 44] were also modulated after MPB treatment. We also found that MPB mediated CHOP activation led to ROS generation

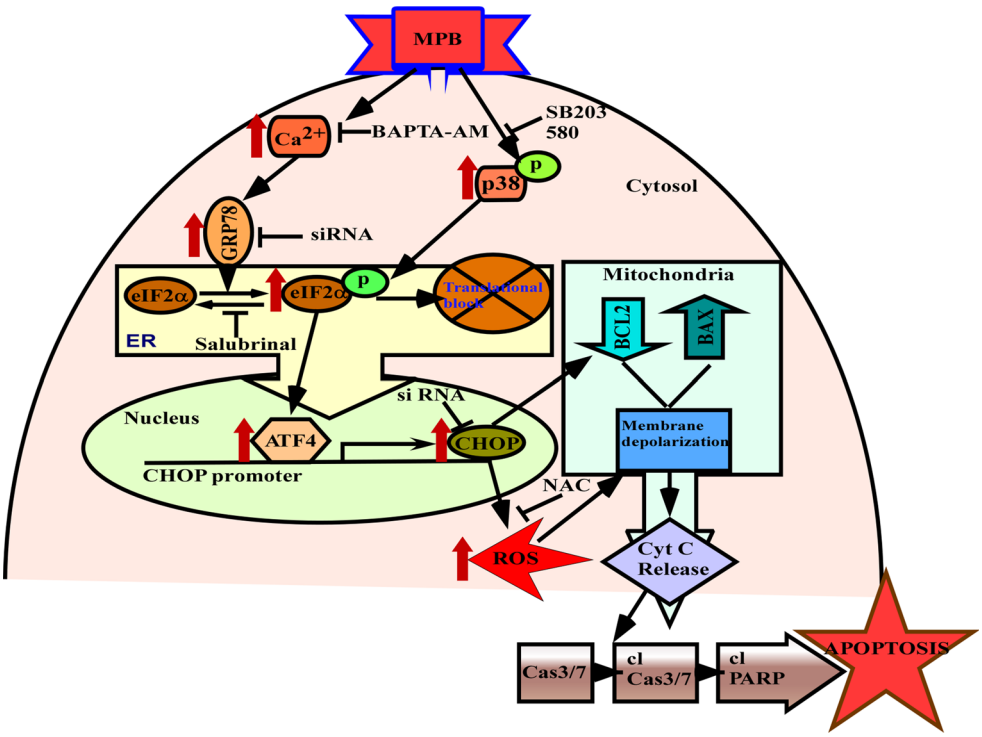

Fig. 9 Proposed model showing the mechanism of action of mephebrindole leading to apoptosis in MCF-7 cells. Based on the findings above model have been proposed showing the role of the mephebrindole in inducing apoptosis in breast cancer through, intracellular calcium hike, phosphop38 activation, ER stress and up-regulation of CHOP by ATF4 induction via phospho eIF2α

which is the necessary signals to induce apoptosis in MCF-7 cells. Our in vitro findings were also supported by our in vivo results where significant tumor regression was observed in EAC bearing Swiss albino allograft mice models. Preceding results thus supported the idea that eIF2α phosphorylation need to be finely tuned to ensure proper maintenance of ER function Immediately after an insult by MPB, eIF2α is transiently phosphorylated to trigger on the adaptation UPR mechanism by inducing ATF4 and CHOP. But simultaneously p38 activation by MPB prolonged the effect of CHOP activation which induced the ROS production and BCL-2 down-regulation followed by apoptosis induction in MCF-7 cells. Thus MPB can be suggested as a suitable candidate for therapeutic development for treatment of patients with breast cancer.

Conclusion

Our findings thus significantly point at the fact that MPB promotes prolonged ER stress development which when coupled with simultaneous p38 activation facilitates apoptotic induction in human breast cancer cells. Our observations from in vitro studies were also validated in in vivo mice models. Hence MPB may be used as a improved therapeutic approach for treatment of breast cancer.

Acknowledgments We are thankful to Prof. Tamara Lah and Dr. Neža Podergajs, National Institute of Biology, Ljubljana, Slovenia for kindly gifting us the MCF 10A cell line. Thanks are due to A. Basu, R. Dutta and K. Das for technical help. This work was supported by the grants from Department of Atomic Energy, Gov't of India. Authors acknowledge Bose Institute and The Center for Research in Nanoscience and Nanotechnology, University of Calcutta, for providing some instrumental facilities. SC thanks DBT for the RGYI Grant BT/PR6627/GBD/27/440/2012.

Authors contributions SC, SG, BB, and PCS conceived the study and designed the experiments. SC, SG, BB, AS, JB performed the experiments. SC, AA, SC, AKM analyzed the data and prepared the figures. SC and SG wrote the paper. PCS supervised the study and revised the manuscript. All authors read and approved the final manuscript.

Compliance with ethical standards

Conflict of interest The authors declare that they have no competing interests.

References

1. Vandewynckel Y-P, Laukens D, Geerts A et al (2013) The paradox of the unfolded protein response in cancer. Anticancer Res 33:4683–4694
2. Xu C, Bailly-Maitre B, Reed JC (2005) Endoplasmic reticulum stress: cell life and death decisions. J Clin Investig 115: 2656–2664
3. Verfaillie T, Garg AD, Agostinis P (2013) Targeting ER stress induced apoptosis and inflammation in cancer. Cancer Lett 332:249–264
4. Hetz C (2012) The unfolded protein response: controlling cell fate decisions under ER stress and beyond. Nat Rev Mol Cell Biol 13:89–102
5. Walter P, Ron D (2011) The unfolded protein response: from stress pathway to homeostatic regulation. Science 334:1081–1086
6. Wang S, Kaufman RJ (2012) The impact of the unfolded protein response on human disease. J Cell Biol 197:857–867
7. Harding HP, Zyryanova AF, Ron D (2012) Uncoupling proteostasis and development in vitro with a small molecule inhibitor of the pancreatic endoplasmic reticulum kinase, PERK. J Biol Chem 287:44338–44344
8. Scheuner D, Song B, mcewen E et al (2001) Translational control is required for the unfolded protein response and in vivo glucose homeostasis. Mol Cell 7:1165–1176
9. Hai TW, Liu F, Coukos WJ, Green MR (1989) Transcription factor ATF cdna clones: an extensive family of leucine zipper proteins able to selectively form DNA-binding heterodimers. Genes Dev 3:2083–2090
10. Lu PD, Harding HP, Ron D (2004) Translation reinitiation at alternative open reading frames regulates gene expression in an integrated stress response. J Cell Biol 167:27–33
11. Vattem KM, Wek RC (2004) Reinitiation involving upstream orfs regulates ATF4 mrna translation in mammalian cells. Proc Natl Acad Sci USA 101:11269–11274
12. Fornace AJ Jr, Alamo I Jr, Hollander MC (1988) DNA damage-inducible transcripts in mammalian cells. Proc Natl Acad Sci USA 85:8800–8804
13. Ma Y, Brewer JW, Diehl JA, Hendershot LM (2002) Two distinct stress signaling pathways converge upon the CHOP promoter during the mammalian unfolded protein response. J Mol Biol 318:1351–1365
14. Ron D, Habener JF (1992) CHOP, a novel developmentally regulated nuclear protein that dimerizes with transcription factors C/EBP and LAP and functions as a dominant-negative inhibitor of gene transcription. Genes Dev 6:439–453
15. Nachshon-Kedmi M, Yannai S, Haj A, Fares FA (2003) Indole-3-carbinol and 3,3′-diindolylmethane induce apoptosis in human prostate cancer cells. Food Chem Toxicol 41:745–752
16. Weng J-R, Tsai C-H, Kulp SK, Chen C-S (2008) Indole-3-carbinol as a chemopreventive and anti-cancer agent. Cancer Lett 262:153
17. De Santi M, Galluzzi L, Lucarini S et al (2011) The indole-3-carbinol cyclic tetrameric derivative ctet inhibits cell proliferation via overexpression of p21/CDKN1A in both estrogen receptor-positive and triple-negative breast cancer cell lines. Breast Cancer Res 13:R33
18. Yean D, W-r Chao, Green C, Jong L (2007) SR13668: a novel dietary indole analog blocks growth factor-stimulated Akt activation and cell proliferation in various cancer cell lines. Cancer Res 67:3364
19. Sharma DK, Rah B, Lambu MR et al (2012) Design and synthesis of novel N, N[prime or minute]-glycoside derivatives of 3,3[prime or minute]-diindolylmethanes as potential antiproliferative agents. Medchemcomm 3:1082–1091
20. Firouzabadi H, Iranpoor N, Khoshnood A (2007) Aluminum tris (dodecyl sulfate) trihydrate Al(DS)3·3H2O as an efficient Lewis acid–surfactant-combined catalyst for organic reactions in water: efficient conversion of epoxides to thiiranes and to amino alcohols at room temperature. J Mol Catal A 274:109–115

21. Robinson JA, Jenkins NS, Holman NA, Roberts-Thomson SJ, Monteith GR (2004) Ratiometric and nonratiometric Ca2+ indicators for the assessment of intracellular free Ca2+ in a breast cancer cell line using a fluorescence microplate reader. J Biochem Biophys Methods 58:227–237
22. Brewis IA, Morton IE, Mohammad SN, Browes CE, Moore HD (2000) Measurement of intracellular calcium concentration and plasma membrane potential in human spermatozoa using flow cytometry. J Androl 21:238–249
23. Vines A, mcbean GJ, Blanco-Fernandez A (2010) A flow-cytometric method for continuous measurement of intracellular Ca(2+) concentration. Cytom A 77:1091–1097
24. Ghosh S, Adhikary A, Chakraborty S et al (2012) Nifetepimine, a Dihydropyrimidone, Ensures CD4(+) T Cell Survival in a Tumor Microenvironment by Maneuvering Sarco(endo)plasmic Reticulum Ca(2+) atpase (SERCA). J Biol Chem 287:32881–32896
25. Chen T, Wong Y-S (2009) Selenocystine induces caspase-independent apoptosis in MCF-7 human breast carcinoma cells with involvement of p53 phosphorylation and reactive oxygen species generation. Int J Biochem Cell Biol 41:666–676
26. Cruickshanks N, Tang Y, Booth L, Hamed H, Grant S, Dent P (2012) Lapatinib and obatoclax kill breast cancer cells through reactive oxygen species-dependent endoplasmic reticulum stress. Mol Pharmacol 82:1217–1229
27. Majumdar SK, Valdellon JA, Brown KA (2001) In vitro investigations on the toxicity and cell death induced by tamoxifen on two non-breast cancer cell types. J Biomed Biotechnol 1:99–107
28. Suberu JO, Romero-Canelón I, Sullivan N, Lapkin AA, Barker GC (2014) Comparative cytotoxicity of artemisinin and cisplatin and their interactions with chlorogenic acids in mcf7 breast cancer cells. ChemMedChem 9:2791–2797
29. Wang S, Konorev EA, Kotamraju S, Joseph J, Kalivendi S, Kalyanaraman B (2004) Doxorubicin induces apoptosis in normal and tumor cells via distinctly different mechanisms: intermediacy of H_2O_2- and P53-dependent pathways. J Biol Chem 279:25535–25543
30. Wozniak K, Kolacinska A, Blasinska-Morawiec M et al (2007) The DNA-damaging potential of tamoxifen in breast cancer and normal cells. Arch Toxicol 81:519–527
31. Travers KJ, Patil CK, Wodicka L, Lockhart DJ, Weissman JS, Walter P (2000) Functional and genomic analyses reveal an essential coordination between the unfolded protein response and ER-associated degradation. Cell 101:249–258
32. Jiang HY, Wek RC (2005) Phosphorylation of the alpha-subunit of the eukaryotic initiation factor-2 (eif2alpha) reduces protein synthesis and enhances apoptosis in response to proteasome inhibition. J Biol Chem 280:14189–14202
33. Kim R, Emi M, Tanabe K, Murakami S (2006) Role of the unfolded protein response in cell death. Apoptosis Int J Program Cell Death 11:5–13
34. Boyce M, Bryant KF, Jousse C et al (2005) A selective inhibitor of eif2alpha dephosphorylation protects cells from ER stress. Science 307:935–939
35. Drexler HC (2009) Synergistic apoptosis induction in leukemic cells by the phosphatase inhibitor salubrinal and proteasome inhibitors. PLoS One 4:e4161
36. Wada T, Penninger JM (2004) Mitogen-activated protein kinases in apoptosis regulation. Oncogene 23:2838–2849
37. Zarubin T, Han J (2005) Activation and signaling of the p38 MAP kinase pathway. Cell Res 15:11–18
38. Ghosh AP, Klocke BJ, Ballestas ME, Roth KA (2012) CHOP potentially co-operates with FOXO3a in neuronal cells to regulate PUMA and BIM expression in response to ER stress. PLoS One 7:e39586
39. Enyedi B, Varnai P, Geiszt M (2010) Redox state of the endoplasmic reticulum is controlled by Ero1L-alpha and intraluminal calcium. Antioxid Redox Signal 13:721–729
40. Mccullough KD, Martindale JL, Klotz LO, Aw TY, Holbrook NJ (2001) Gadd153 sensitizes cells to endoplasmic reticulum stress by down-regulating BCL-2 and perturbing the cellular redox state. Mol Cell Biol 21:1249–1259
41. Berridge MJ, Lipp P, Bootman MD (2000) The versatility and universality of calcium signalling. Nat Rev Mol Cell Biol 1:11–21
42. Mattson MP, Chan SL (2003) Calcium orchestrates apoptosis. Nat Cell Biol 5:1041–1043
43. Orrenius S, Zhivotovsky B, Nicotera P (2003) Regulation of cell death: the calcium-apoptosis link. Nat Rev Mol Cell Biol 4:552–565
44. Puthalakath H, O'Reilly LA, Gunn P et al (2007) ER stress triggers apoptosis by activating BH3-only protein Bim. Cell 129:1337–1349